Nanoscale

Cite this: *Nanoscale*, 2012, **4**, 7250

www.rsc.org/nanoscale

PAPER

Evaluation of piezoelectric property of reduced graphene oxide (rGO)–poly(vinylidene fluoride) nanocomposites

Alamusi,[a] JunMin Xue,[b] LiangKe Wu,[a] Ning Hu,*[a] Jianhui Qiu,[c] Christiana Chang,[d] Satoshi Atobe,[e] Hisao Fukunaga,[e] Tomonori Watanabe,[a] YaoLu Liu,[a] HuiMing Ning,[a] JinHua Li,[a] Yuan Li[f] and Yinghua Zhao[g]

Received 8th August 2012, Accepted 25th September 2012
DOI: 10.1039/c2nr32185h

We improved the piezoelectric property of poly(vinylidene fluoride) (PVDF) by employing graphene. The reduced graphene oxide (rGO)–PVDF nanocomposites were prepared by a solution casting method and the rGO contents ranged from 0.0 wt% to 0.2 wt%. To induce the piezoelectric β-phase crystal structure, the nanocomposite films were drawn in a ratio of 4–5 and polarized by a step-wise poling method. To evaluate the piezoelectric property, the output voltages of the rGO–PVDF nanocomposite films were measured through extensive experimental vibration tests. The experimental results show that the rGO–PVDF nanocomposite film with 0.05 wt% rGO loading possesses the highest output voltage compared with other loadings, which is around 293% of that of the pure PVDF film. Moreover, it can be found that with the increase of the rGO content from 0 wt% to 0.2 wt%, the output voltage tends to have a peak at 0.05 wt%. The main reason for this phenomenon is that a more β-crystalline phase can be formed at those rGO loadings, as confirmed by XRD and FT-IR spectrum analyses.

Introduction

Due to their excellent piezoelectric and ferroelectric properties, poly(vinylidene fluoride) (PVDF) and its copolymers have been intensively investigated by many researchers and are considered to be promising materials for making low-cost sensors in a variety of fields, such as structural vibration control and various measurements applications.[1–5] Moreover, it is promising to use this material in environmental energy harvesting to transform mechanical energy into electrical energy due to its high ductility, high applicability to curved structures, advantage of free adjustment of sizes, *etc.* However, due to its low coupling between electrical and mechanical properties and its relatively low generated voltage and force, the potential of PVDF in piezoelectric sensor/actuator and energy harvesting applications is still limited.

To improve PVDF's electro-mechanical coupling, a number of carbon based nanoparticles, such as carbon nanotubes (CNTs), have been proposed to alter the polymer microstructure and promote piezoelectricity. Ramaratnam and Jalili blended single-walled carbon nanotubes (SWCNTs) and multi-walled carbon nanotubes (MWCNTs) with PVDF at 0.5 wt% addition to fabricate piezoelectric strain sensors with improved properties.[6] Lee *et al.* used MWCNTs as fillers in PVDF and studied the resulting changes in the PVDF crystal structure before and after the drawing and poling processes.[7] It was found that the addition of CNTs increased nucleation of the piezoelectric β-phase of PVDF, improving the piezoelectric properties of the polymer before drawing. Increases in the piezoelectric strain constant, d_{31}, were observed post-drawing and poling without detriment to the elastic modulus, though a peak in d_{31} occurs at approximately 0.2% CNT content by weight, indicating that d_{31} is sensitive to the CNT content and careful control of composite composition is needed to maximize the piezoelectric properties. Sun conducted an extensive study on the use of carbon black (CB) in a hybrid high-density polyethylene (HDPE)–PVDF composite fiber for use as a piezoelectric textile actuator.[8] Like CNTs, CB was found

[a]*Department of Mechanical Engineering, Chiba University, 1-33 Yayoi-chio, Inage-ku, Chiba City, Chiba 263-8522, Japan. E-mail: huning@faculty.chiba-u.jp; alamusi@chiba-u.jp; Fax: +81-43-290-3204; Tel: +81-43-290-3204*
[b]*Department of Materials Science, National University of Singapore, 21 Lower Kent Ridge Road, Singapore 119077. E-mail: msexuejm@nus.edu.sg*
[c]*Department of Machine Intelligence and Systems Engineering, Akita Prefectural University, Akita 015-0055, Japan. E-mail: qiu@akita-u.ac.jp*
[d]*Department of Mechanical Engineering, University of Houston, Houston, TX, USA. E-mail: cchang2@uh.edu*
[e]*Department of Aerospace Engineering, Tohoku University, 6-6-01 Aramaki-Aza-Aoba, Aoba-ku, Sendai 980-8579, Japan. E-mail: atobe@ssl.mech.tohoku.ac.jp; fukunaga@ssl.mech.tohoku.ac.jp*
[f]*Department of Nanomechanics, Tohoku University, 6-6-01 Aramaki-Aza-Aoba, Aoba-ku, Sendai 980-8579, Japan. E-mail: liyuan@ism.tohoku.ac.jp*
[g]*Institute of Road and Bridge Engineering, Dalian Maritime University, Dalian 110015, P.R. China. E-mail: yhzhao@dlmu.edu.cn*

to greatly increase the fibers' piezoelectric constant as compared to neat polymer fibers through increased nucleation of the PVDF β-phase. An optimized composite was used to design a synthetic muscle fiber with a cross-section of 26 mm^2 actuated at 4.5 V, producing an actuation force of 0.5 N, sufficient to flex a human finger joint. With the demonstrated improvements in electro-mechanical coupling properties, carbon nanoparticle based PVDF composites show greater potential in sensing and actuating applications.

However, these results are still limited by the performance of the selected filler materials. It is well-known that graphene possesses a unique atomic structure which leads to its excellent mechanical, thermal, electrical and optical properties.[9,10] Furthermore, recent studies have shown that there are techniques to grow high-quality graphene cheaply and that graphene demonstrates better biocompatibility than CNTs, making it significantly more attractive for commercial and industrial applications.[11,12] However, to date, there is no research in the literature regarding the study of piezoelectric properties of reduced graphene oxide (rGO)–PVDF nanocomposites.

Thus, to improve the piezoelectric properties of PVDF, in this study, rGO was employed as a filler in PVDF and was combined with the proper drawing and poling processes to make rGO–PVDF nanocomposite films which have potential application in sensing and actuation. The piezoelectric properties of these nanocomposite films, as affected by the influence of rGO addition and the drawing and poling processes, were studied through a series of vibration tests. Finally, to uncover the mechanisms of the improved piezoelectric properties of this nanocomposite film, XRD and FT-IR spectral analyses and polarized optical microscopy (POM) imaging were performed to study the films' internal crystal structure.

Experimental procedure

Sample preparation

Preparation of rGO. rGO was prepared by oxidation of natural flake graphite powder using a modified Hummers method. In a typical synthesis, 1 g graphite powder and 1 g $NaNO_3$ were mixed, and then added to 46 ml concentrated H_2SO_4 (98%) in an ice bath. After magnetically stirring for 1 hour, 6 g $KMnO_4$ was gradually added to the mixture under stirring. The mixture was then transferred to a water bath of 35 °C for 1 day. Successively, 40 ml H_2O was slowly added to the mixture, during which the temperature of the mixture rose to around 80 °C. Finally, 100 ml H_2O followed by 20 ml 20% H_2O_2 solution was added to the mixture, and the mixture was further stirred for 30 min. The intermediate product GO was collected by centrifugation, and was repeatedly rinsed with 4% HCl solution followed by de-ionized water. After that, the oxidized graphite was dried in an oven at 70 °C for 4 days. An appropriate amount of GO was dispersed in ethylene glycol (EG) by ultrasonication. The mixture was then transferred to a 125 ml Teflon-lined stainless steel autoclave and solvothermally treated in an air-flow electric oven at 200 °C for 4 days. The final product rGO was collected by centrifugation and washed with pure ethanol for 3 times.

The obtained graphene flakes were observed by transmission electron microscopy (TEM, JEOL 100CX instrument) as shown in Fig. 1. From Fig. 1, it can be found that some flakes are composed of 2–4 individual graphene sheets, and some others may be composed of 15–25 individual sheets. Fig. 2 shows a typical atomic force microscopy (AFM) image (AFM, Veeco NanoScope IV Multi-Mode with the tapping mode) of a single piece exfoliated GO sheet with a size around 5 μm. The average thickness of the as-prepared GO sheet was around 1.034 nm, which was slightly larger than the theoretical value of 0.78 nm for single layer graphene. The additional thickness might have arose from the oxygen-containing groups such as epoxy and hydroxyl groups on the GO surface.

Preparation of the rGO–PVDF nanocomposite film. PVDF powder and *N*,*N*-dimethylformamide (DMF) were purchased from Tokyo Zairyo Co., Ltd., Japan and Wako Pure Chemical Industries Co., Ltd., Japan, respectively. Based on the different contents of rGO, seven kinds of rGO–PVDF nanocomposite films were fabricated by the solution casting method. The films contained different rGO contents, consisting of 0 wt%, 0.01 wt%, 0.02 wt%, 0.03 wt%, 0.05 wt%, 0.1 wt%, and 0.2 wt% rGO loadings, respectively. The detailed procedures are described as follows:

(1) rGO was dispersed into a melting agent, DMF, by using an ultrasound dispersion machine during three 30 min cycles.

(2) PVDF powder was poured into the mixture solution and then the solution was stirred using a planetary centrifugal mixer at 2000 rpm for 10 min. The mass ratio was (rGO + PVDF) : DMF = 1 : 3.

(3) The rGO–PVDF–DMF mixture solution was sonicated for 5 min and mechanically stirred using the planetary centrifugal mixer at 2000 rpm for 10 min and then defoamed for 1 min.

(4) The final mixture was poured onto an aluminum plate and was made into thick films in a detachable mould (12 × 60 × 0.25 cm). Then, the aluminum plate was heated to 90 °C for

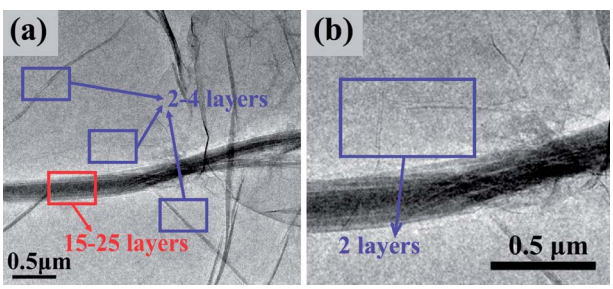

Fig. 1 (a) TEM image of the obtained rGO. (b) Image of central enlargement of (a).

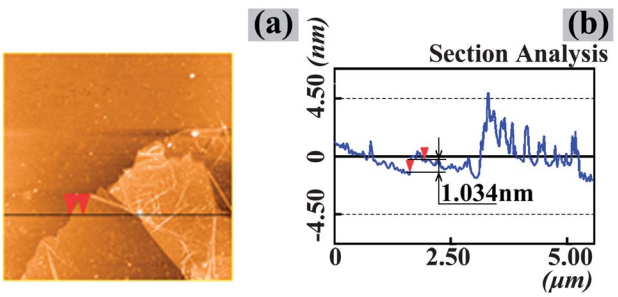

Fig. 2 AFM image of the obtained rGO sheet with height profile.

removing the DMF. After drying, uniform rGO–PVDF thick films were obtained.

(5) The films were stretched using a universal testing machine. The drawing rate was 10 mm min^{-1}, and the final elongation was 400–500% at around 60 °C. The pictures of the rGO–PVDF nanocomposite films before and after drawing are shown in Fig. 3.

(6) After drawing, the poling process was carried out by a step-wise poling method[13] illustrated in Fig. 4. In the step-wise poling method, step-by-step rising voltages were applied to the films in silicone oil at room temperature. In this study, the poling interval was 8 min, the pause time was 4 min, and the number of steps was set to 5. It should be noted that the addition of graphene is beneficial to increasing the poling voltage, which leads to higher piezoelectric properties. Here, for comparison, we used 60 MV m^{-1} as the same maximum applied electric field for all samples.

Test procedures

In order to evaluate the piezoelectric property of the aforementioned rGO–PVDF nanocomposite films, specimens of different rGO loadings, *i.e.*, 0 wt%, 0.01 wt%, 0.02 wt%, 0.03 wt%, 0.05 wt%, 0.1 wt%, and 0.2 wt% were attached to the surface of a cantilever aluminum beam to measure the output voltages while the beam was in vibration. The size of a specimen is 30 mm × 30 mm. At the free-end of the beam, an electromagnet device was used to excite vibration motion.

The standard amplitude of the vibration was 1 mm for low frequencies (5, 20 and 30 Hz). Moreover, at high frequency (120 Hz), the standard amplitude of the vibration was 1 μm. The dimensions of the cantilever beam are schematically depicted in Fig. 5a and 6. To prevent the discharge of the electrodes of the nanocomposite film when it was directly attached to the conductive aluminum beam, the beam was coated with an epoxy resin insulating layer before adhering to the nanocomposite films. The apparatus used for measurement is illustrated schematically in Fig. 6. In this work, the cantilever beam was excited by the electromagnet. The excitation signal was produced by a function generator and applied to the electromagnet through a voltage amplifier. The excitation frequencies of the sinusoidal functions were 5, 20, 30 and 120 Hz, respectively, avoiding the first three resonant frequencies of the test specimen. Voltage changes of the nanocomposite films were measured using an oscilloscope connected to a PC. In addition, the collected voltage data were de-noised using a band-pass filter in the PC. During this process, the displacements of the aluminum beam tip were also measured using a laser displacement sensor for calibration.

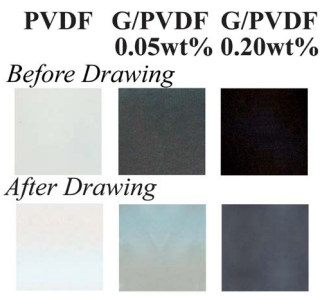

Fig. 3 rGO–PVDF nanocomposite films before and after drawing (G–PVDF:rGO–PVDF nanocomposite).

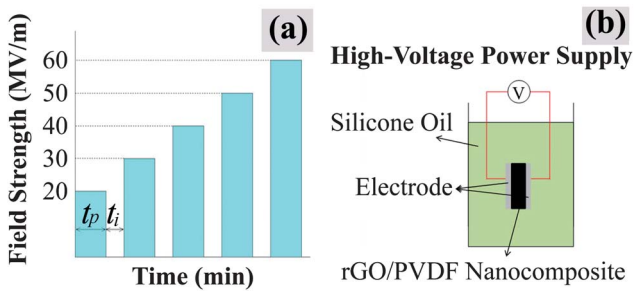

Fig. 4 Description of the poling procedure: (a) schematic diagram of the step-wise poling technique (poling time t_p: 8 min; pause time t_i: 4 min) and (b) schematic illustration of the step-wise poling setup.

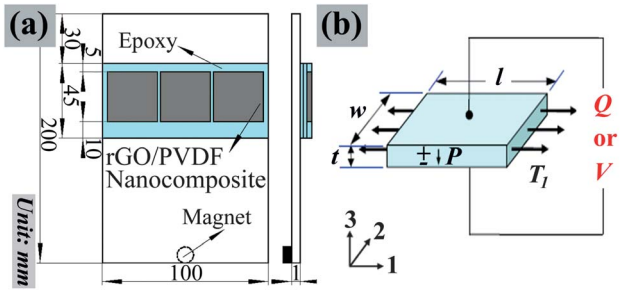

Fig. 5 Schematic illustration of rGO–PVDF nanocomposite samples: (a) dimensions of samples (3 pieces) and beam and (b) the relationship between charge and stress on a piezoelectric film.

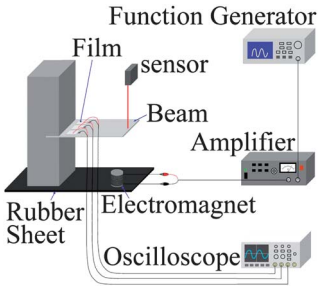

Fig. 6 Experimental setup used to evaluate the open-circuit voltage of nanocomposite.

Results and discussion

Output voltage results

Table 1 shows the maximum output voltage of the samples with different rGO loadings (*i.e.*, 0.0 wt%, 0.05 wt%, and 0.2 wt%) at some excitation frequencies (5, 20, 30, and 120 Hz). The maximum output voltage of the 0.05 wt% sample at each frequency and the percentage voltage increase of each sample at each frequency, the relationship between time and output voltage of the 0.05 wt% sample of at 30 Hz frequency are shown in Fig. 7–9, respectively. Note that the maximum voltage outputs for all the samples occur at 30 Hz frequency.

Table 1 Maximum output voltage of rGO–PVDF nanocomposite films at various rGO loadings

Graphene loadings (wt%)		0.00	0.05	0.20
Maximum output voltage (V)	5 Hz	0.45	0.86	0.81
	20 Hz	0.63	1.61	1.25
	30 Hz	1.12	3.28	3.00
	120 Hz	0.40	0.79	0.73

From Table 1, it can be found that the rGO–PVDF nanocomposite film with 0.05 wt% loading has the highest output voltage at each excitation frequency and the output voltage is between 191% (5 Hz) and 293% (30 Hz) compared to the pure PVDF film, as shown in Fig. 7. Particularly, when the excitation frequency is 30 Hz, the output voltage increases to approximately 293% compared to the pure PVDF film.

The output voltage V can be obtained from the relationship between the charge and stress (Fig. 5b) as follows:

$$V = \frac{Q}{C} = \frac{T_1 d_{31} t}{\varepsilon_{33}} = E' \varepsilon' g_{31} t = E' t g_{31} \times \frac{\Delta l}{l} \quad (1)$$

where Q is the saved charge, C is the film electric capacitance, T_1 is the stress along the 1 direction, ε_{33} is the permittivity of the film without stress, E' is the Young's modulus of the film, ε' is the strain along the 1 direction, Δl is the elongation along the 1 direction, g_{31} is the piezoelectric voltage constant, and d_{31} is the piezoelectric strain constant.

From eqn (1), the remarkable increase of output voltages due to addition of rGO implies the significant increase of the piezoelectric voltage constant g_{31} under the assumption that there is no obvious variation in the Young's modulus E' of the film since the maximum addition of rGO is 0.2 wt%. Furthermore, the piezoelectric voltage constant g_{31} is related to the piezoelectric strain constant d_{31} as: $g_{31} = d_{31}/\varepsilon_{33}$. Under the assumption that the permittivity ε_{33} of the film without stress is not influenced significantly by the addition of rGO, it can be estimated that the piezoelectric strain constant d_{31} increases remarkably, *e.g.*, 1–2 times increases (Fig. 7 and 8). This result is much higher than many previously reported data.[7,14,15] For instance, Lee *et al.* identified that the maximum increase of d_{31} of PVDF is around 10% at an optimal addition of MWCNT, *i.e.*, 0.2 wt%.[7] Kim *et al.* indicated that the d_{33} of the MWCNT–PVDF nanocomposite increases only 15% of that of pure PVDF.[14] Levi *et al.* argued that the piezoelectric response of the PVDF–TrFE–HiPCo–SWCNT nanocomposite increases around 18% compared to the PVDF–TrEE nanocomposite.[15]

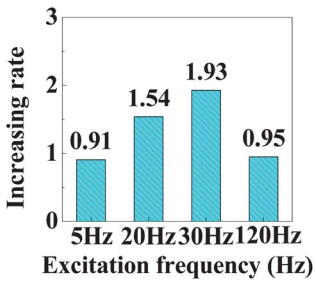

Fig. 7 Increasing rate of output voltages of rGO–PVDF nanocomposite films in the rGO loading of 0.05 wt%.

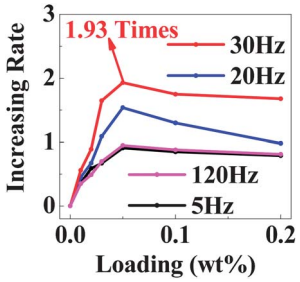

Fig. 8 Increasing rate of output voltages of rGO–PVDF nanocomposite films.

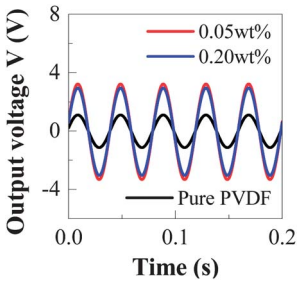

Fig. 9 Output voltages of rGO–PVDF nanocomposite films (0.0 wt%, 0.05 wt%, and 0.2 wt%, 30 Hz).

Moreover, from Fig. 8, it can be found that as the rGO content increases from 0 wt% to 0.2 wt%, the output voltage appears to have a peak at 0.05 wt%. This implies that with the increase of rGO content, the output voltage tends to have peak of output voltages in each frequency. The directly measured signals of various films are shown in Fig. 9, which indicates that, compared with the pure PVF films, the rGO–PVDF nanocomposite films (0.05 wt% and 0.2 wt%) with much higher amplitudes show good responsiveness and traceability to the excitation and that there is promise for strain sensor applications.

Moreover, there is no obvious phase shift among three signals, which implies that the influence of small rGO contents on the film stiffness may be minor. Because the crystal structure of a polymer nanocomposite can affect its piezoelectric performance, the more the β-crystalline phase is present, the better the piezoelectric performance of the material. From the above results, it can be found that the output voltage of nanocomposite films increases with the addition of rGO. To explain this phenomenon, several analyses were carried out to study the crystal structures in the nanocomposite films.

X-Ray diffraction analysis

X-Ray Diffraction (XRD) equipment (MPX 3A of MAC Science Co., Ltd. Japan) was employed to analyze the rGO–PVDF nanocomposite films. For XRD analysis, the samples before and after the uniaxial drawing with different rGO loadings were measured. Note that none of the samples were treated by poling. The measurement speed was 1 deg min^{-1}, and the measurement range was 10–30 deg. The XRD results are shown in Fig. 10.

Fig. 10a describes the XRD results for rGO–PVDF nanocomposite films before the drawing process. It can be found that

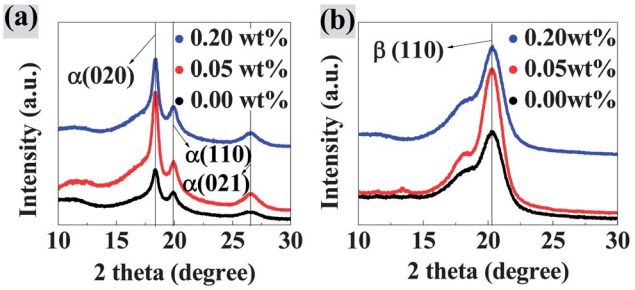

Fig. 10 XRD patterns of rGO–PVDF nanocomposites: (a) before drawing and (b) after drawing.

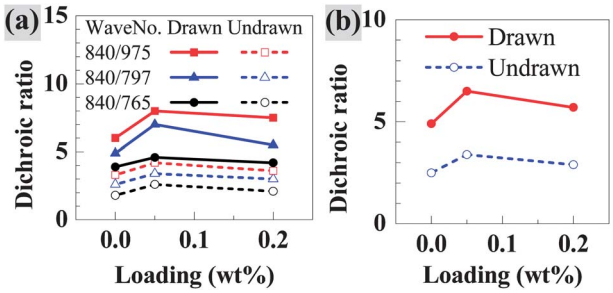

Fig. 12 Dichroic ratio of rGO–PVDF nanocomposites: (a) before drawing and (b) after drawing.

three characteristic diffraction peaks are observed at the diffraction angles (2θ): 18.4°, 19.9° and 26.5°, which are assigned to (020), (110), and (021) crystal plane reflections of the α form chain. Fig. 10b shows the XRD results of the samples after drawing. In this figure, only one high peak can be observed at 2θ (theta) = 20.6° corresponding to (110) of the β-phase. However, the peaks corresponding to the α-phase crystal have disappeared. This indicates that the uniaxial drawing process can induce a remarkable transition from α-type crystal to β-phase crystal in the rGO–PVDF nanocomposite films. In addition, after the uniaxial drawing process, the rGO–PVDF nanocomposite film with rGO 0.05 wt% loading can also be confirmed to possess the highest relative peak intensity at $2\theta = 20.6°$, compared with the platform in Fig. 10b.

FT-IR spectral analysis

In order to further investigate the crystal structure of the nanocomposite films, FT-IR spectral analysis were carried out. The thickness of the samples for FT-IR spectral analysis was 10 μm. The spectra were recorded in the region between 1400 and 600 cm^{-1}, with a spectral resolution of 4 cm^{-1} and an aperture of 25 × 100 μm. For each spectrum, 50 scans were averaged. Generally, the corresponding IR absorption band characteristics of α-phase crystal appear at 615, 765, 797, and 975 cm^{-1}, whereas for β-phase peaks in IR the spectra are located at 840 and 1280 cm^{-1}. It can be found from Fig. 11a that the α-phase crystal certainly exists in the rGO–PVDF nanocomposite films with various rGO loadings before drawing. Nonetheless, from Fig. 11b, we can see that β-phase crystal peaks increase significantly at 840 and 1280 cm^{-1}, while the peaks corresponding to the α-phase crystal decrease, with some even disappearing after drawing. This

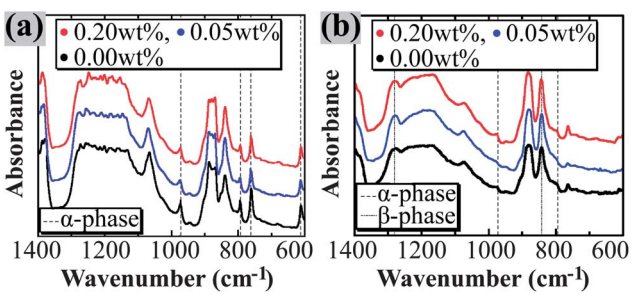

Fig. 11 FT-IR spectra of rGO–PVDF nanocomposites: (a) before drawing and (b) after drawing.

indicates that α-phase crystal peaks were transformed to β-phase crystal peaks by drawing, which is consistent with the results of XRD analysis.

As shown in Fig. 12, the dichroic ratio, which was obtained by dividing the intensity of β-phase crystal by that of α-phase crystal in Fig. 11, was employed to quantitatively analyze the relative amount of the crystal structures in the nanocomposite films.

Fig. 12a shows the dichroic ratio of the β-phase crystal peak at 840 cm^{-1} *versus* each α-phase crystal peak at 765, 797, and 975 cm^{-1}, respectively. Fig. 12b shows the average dichroic ratio of the β-phase crystal peak *versus* the α-phase crystal peak. It can be seen that the relative amount of the β-phase crystal peak *versus* the α-phase crystal peak in all rGO–PVDF nanocomposites increases after drawing. This means that the drawing process can lead to the transition from the α-phase crystal peak to the β-phase crystal peak. However, the dichroic is almost constant for any rGO loading before drawing (Fig. 12a and b), indicating that the addition of rGO has a minor effect on the β-phase crystal before drawing. However, for the samples after drawing (Fig. 12a and b), the relative amount of β-phase crystal *versus* α-phase crystal varies markedly with the content of rGO. It increases with the content of rGO initially, reaches the maximum value at 0.05 wt%, and then decreases as the rGO content increases up to 0.2 wt%. This indicates that the content of rGO may influence the transformation of the α-phase crystal to the β-phase crystal in the drawing process. This phenomenon is consistent with the output voltages what we observed in the vibrating tests.

The reason for this behavior may be that up to 0.05 wt% rGO content, the β-phase crystal slightly increased due to the role of rGO as nuclei for rapid crystallization before drawing (Fig. 12a and b). Or, perhaps more α-phase crystals may be formed due to the addition of 0.05 wt% rGO (Fig. 10a), and then more β-phase crystals can be generated by the drawing process (Fig. 10b). However, higher contents of rGO (over 0.05 wt%) could act as a hindrance for initial crystallization of the α-phase (Fig. 10a) or the β-phase. Moreover, this negative effect could be amplified in the drawing process to transform the α-phase crystal into the β-phase crystal by comparing Fig. 12a and b since more rGO with high stiffness may restrict the tensional deformation of crystals, leading to the weak phase transformation.

Polarized optical microscopy observation

Fig. 13 shows the polarized optical microscopy (POM) images of pure PVDF and various rGO–PVDF nanocomposite films

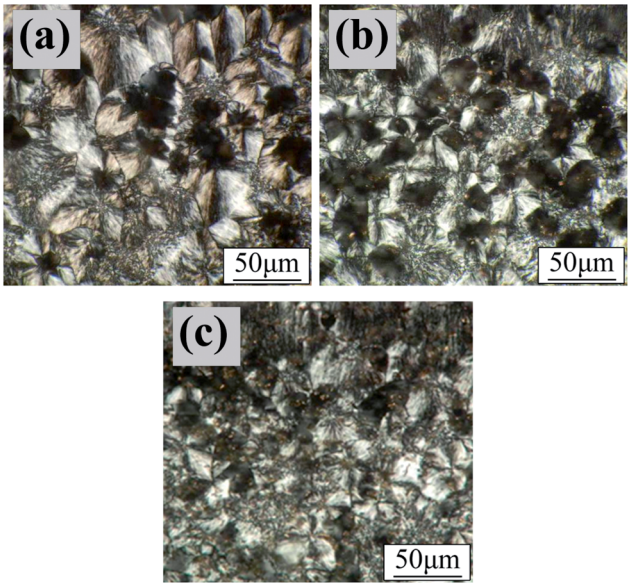

Fig. 13 POM images of rGO–PVDF nanocomposites before drawing: (a) 0.00 wt%, (b) 0.05 wt%, and (c) 0.20 wt%.

before drawing, respectively. It can be found that the crystalline morphologies of PVDF nanocomposites are quite different after adding rGO. In Fig. 13a, the POM image exhibits a number of well-developed spherulites with typical Maltese crosses. By adding 0.05 wt% content of rGO, in Fig. 13b, the number of spherulites increases and the average diameter of spherulites decreases. This indicates that the incorporation of rGO (*e.g.*, 0.05 wt%) increases the amount of heterogeneous nucleation sites in the PVDF matrix and, therefore, enhances crystallization. In Fig. 13c, its crystallinity is slightly lower at 0.2 wt% rGO loading, which means that the initial crystallization may be weakened by the increased loading of rGO. The slightly lower piezoelectric performance in this case of higher filler additions may also be explained by the charge accumulation mechanism as indicated by Kim *et al.*[14] Moreover, with only information from the present examination, including the POM images, at present there are still some inherent factors which are unclear. It should be noted that the crystallinity is also influenced by the fabrication conditions. Therefore, the above observed evidence may be only valid for the fabrication conditions used here, which is the same for all samples.

Conclusions

In this study, we investigated the improvement of the piezoelectric property of rGO–PVDF nanocomposite films. Different contents of rGO (0 wt%, 0.01 wt%, 0.02 wt%, 0.03 wt%, 0.05 wt %, 0.1 wt% and 0.2 wt%) were added to PVDF and combined with a drawing and poling process to improve its piezoelectric performance. To evaluate the performances of the rGO–PVDF nanocomposite films, the output voltages of these rGO–PVDF nanocomposite films in vibration tests were measured and it was found that when the exciting frequency is 30 Hz, the output voltage of the film with 0.05 wt% content was 293% of that of the pure PVDF film, also much higher than that of the CNTs–PVDF nanocomposite film, *etc.* Furthermore, the output voltage tends to have a peak at 0.05 wt%. Through XRD and FT-IR analyses, it was concluded that the lower amount of rGO in the PVDF polymer plays a crucial role in crystallization, thus improving the piezoelectric performance. In this work, the optimal content of rGO was found to be 0.05 wt%.

Notes and references

1 A. J. Lovinger, *Polymer*, 1981, **22**, 412.
2 D. L. Winsor, J. I. Scheinbeim and B. A. Newman, *J. Polym. Sci., Polym. Phys. Ed.*, 1996, **34**, 2967.
3 Z. G. Zeng, G. D. Zhu, L. Zhang and X. J. Yan, *Chin. J. Polym. Sci.*, 2009, **27**, 479.
4 L. Priya and J. P. Jog, *J. Polym. Sci., Part B: Polym. Phys.*, 2003, **41**, 31.
5 Z. B. Qiu, C. Z. Yan, J. M. Lu and W. T. Yang, *Macromolecules*, 2007, **40**, 5047.
6 A. Ramaratnam and N. Jalili, *J. Intell. Mater. Syst. Struct.*, 2006, **17**, 199.
7 J. S. Lee, G. H. Kim, W. N. Kim, K. H. Oh, H. T. Kim, S. S. Hwang and S. M. Hong, *Mol. Cryst. Liq. Cryst.*, 2008, **491**, 247.
8 M. H. Sun, MS thesis, North Carolina State University, 2004.
9 H. Zhao, K. Min and N. R. Aluru, *Nano Lett.*, 2009, **9**, 3012.
10 S. Wang, M. Tambraparni, J. Qiu, J. Tipton and D. Dean, *Macromolecules*, 2009, **42**, 5251.
11 V. Y. Aristov, G. Urbanik, K. Kummer, D. V. Vyalikh, O. V. Molodtsova, A. B. Preobrajenski, A. A. Zakharov, C. Hess, T. Hänke, B. Büchner, I. Vobornik, J. Fujii and G. Panaccione, *Nano Lett.*, 2010, **10**, 992.
12 Y. Chang, S. T. Yang, J. H. Liu, E. Dong, Y. Wang, A. Cao and H. Wang, *Toxicol. Lett.*, 2011, **200**, 201.
13 D. Setiadi, T. D. Binnie, P. Regten and M. Wubbenhorst, in *9th International Symposium on Electrets*, 1996, vol. 9, p. 831.
14 G. H. Kim, S. M. Hong and Y. Seo, *Phys. Chem. Chem. Phys.*, 2009, **11**, 10506.
15 N. Levi, R. Czerw, S. Xing, P. Iyer and D. L. Carroll, *Nano Lett.*, 2004, **4**, 1267.